Smoke Flow Visualizations for the Study of Surface Dielectric Barrier Discharge Induced Flow Field

R. Sriram[1], Srisha Rao M. V.[1], Suparna Pal[2] and G. Jagadeesh[3]
[1]Department of Aerospace Engineering, Indian Institute of Science, Bangalore, India
[2]Defence Research and Development Laboratory, Hyderabad, India
[3]Department of Aerospace Engineering, Indian Institute of Science, Bangalore, India

Abstract

The flow field induced by surface dielectric barrier discharge (SDBD) is visualized using illumination of smoke seeded to the flow. A planar SDBD of 50 mm span is created on a flat surface between thin copper electrodes separated by layers of kepton tapes which act as dielectric; AC voltage of 25 kV (peak to peak) is supplied across the electrodes. The smoke is illuminated by a planar laser sheet, and the time resolved visualizations are captured using a high speed camera operated at a recording rate of 2000 frames per second. The time evolution of the starting vortex and the steady wall jet that eventually gets established on the surface are recorded. The speed of the smoke front at the beginning of actuation and the starting vortex speed are quantified from the visualizations, which are used for parametric study of the SDBD flow actuator. The DBD actuator is found to induce a maximum velocity of 8 m/s close to the electrode at AC frequency of 2000 Hz. It is found that the starting vortex speed increases as the AC frequency is increased, reaching a maximum at 2000 Hz, after which the starting vortex speed decreases. The temporal behaviour of starting vortex with pulsed actuation is also studied and contrasted with the case of quasi steady actuation.

1. INTRODUCTION

Dielectric Barrier Discharge (DBD) plasma actuators are found to be potential candidates for active flow control and a good amount of research efforts are directed towards them through the past decade [1]. Roughly speaking, DBD is the electric discharge between electrodes that are separated by a dielectric medium between them, requiring the application of high AC voltage. The particular aspect of interest concerning flow control has been the body force exerted on the surrounding gas (neutral molecules) by the plasma accelerated by the electric field. This electro-hydrodynamic (EHD) actuation of DBD generates a fluid flow, typically a few meters per second in order. The interest in DBD plasma actuators for aerodynamic flow control is further motivated by their simple construction, fast time response, low power consumption and ease of implementation.

Literature on the use of DBD actuators for controlling low speed flows is quite extensive. The EHD actuation of DBD has been used to control flow separation [2-5]. Some other applications of DBD and related atmospheric pressure plasma actuators include enhancing combustion [6], cavity tone attenuation [7] and jet mixing enhancement [8]. Despite a general belief that the DBD- typically generating fluid velocities of only few meters per second- may not be effective in controlling the high speed flows, a few very recent research efforts have successfully exploited and optimized DBD for high speed flow applications [9,10]. Other possible applications on the modulation of flow stability (which shall possibly be achieved by unsteady actuation) are yet to be realized.

With the control of flow being achieved by the EHD actuation and the consequential displacement of the surrounding fluid, it is important to understand the EHD forces and the disturbance that the forces create on the surroundings. Particularly, from flow control perspective, it is important to know the correlation between the source of EHD forces in DBD (in the form of supply power and its temporal variation) and the actuation, which shall be best quantified by measures of the flow field generated in quiescent air around the DBD actuator. It is with this backdrop that experiments are initiated to get some insight into the nature of the DBD induced flow in quiescent atmosphere. Smoke flow visualizations are carried out using high speed camera to temporally resolve the flow field. Quantitative

measures are established from the visualizations which are then used to study the role of AC frequency and pulsing of the actuation.

2. DIELECTRIC BARRIER DISCHARGE- CONFIGURATION AND MECHANISM

Although DBD actuators can be of many different configurations, the present studies are concerned with typical planar configuration. This is also the configuration almost always used in the literature concerning surface DBD generated flows and flow control. It consists of two electrodes, one exposed to the atmosphere and the other buried under a dielectric, placed below the exposed electrode. Typically the electrodes along with the dielectric are so thin that the entire actuator is almost in flush with the surface. Figure 1 shows a schematic of the actuator, as would be seen from the side. Figure 2 shows schematically the top and front view, explaining various geometric parameters associated with the actuator.

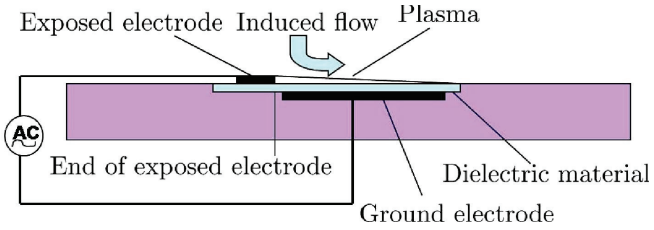

Figure 1. Schematic of DBD actuator as viewed from side

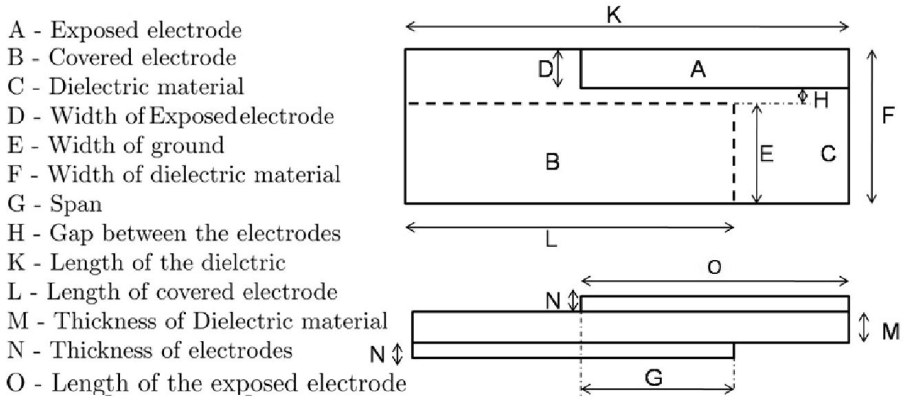

Figure 2. Schematics of DBD actuator as viewed from top and from front

When a high voltage, high frequency AC or pulsed DC is applied across the electrodes, it causes the air to ionize to quasi-neutral plasma which is created on the dielectric surface above the ground electrode. The ionized air appears as a low-intensity, relatively uniform, diffuse purple glow. This emission can be seen with naked eye only in darkened space. Enloe et al. [11] described in detail the mechanism of the DBD actuator. During one half cycle of AC the electrons are supplied from the electrode and during the other half electrons come from the dielectric surface. This accounts for the marked asymmetry between the two half cycles, because of which the net body force exerted on neutral molecules (by the ions drifted by the electric field) is unidirectional when averaged over time, considering that at typically high AC frequencies of DBD the actuation is quasi-steady. Thus there is a wall jet spreading on the surface in the direction from the exposed electrode towards the covered electrode.

Various parameters on which the DBD generated flow depends on have been carefully studied and reported in the literature. These include dielectric thickness and strength, electrode geometry, input voltage and frequency and also the AC waveform [12-15]. PIV of the flow field are also reported in the literature [14, 16]. Many such studies try to correlate the measured reaction force (corresponding to the

generated body force) or a characteristic velocity of the jet against these parameters. Integrating the velocity profiles downstream of the actuator the fluid momentum can be estimated. A consistency between this momentum and the measured reaction force is also verified[14]. A maximum induced velocity of 8 m/s in the wall jet profile was reported [15]. There are also numerical works in the literature simulating the experimentally observed results so as to further understand the physics involved [17-20]. The experimental data on DBD is either used to model the DBD flow in phenomenological fashion so as to incorporate the model in numerical studies on flow control; or if modeled fundamentally using first principles involving complex chemistry and species transport equations coupled with Navier-Stokes equations, the experimental data is obviously required to validate. Recently Whalley and Choi [21] (2010) presented a series of smoke flow visualizations of the wall jet and the starting vortex generated by a single DBD actuator and the collision of starting vortices generated by two oppositely placed DBD actuators in quiescent air. Simple, yet clear, the smoke flow visualizations reveal important qualitative aspects, especially concerning the flow starting. In the present study smoke flow visualizations are extended in quantitative fashion to facilitate the parametric study of DBD. The details of the studies are presented subsequently.

3. EXPERIMENTAL SETUP

A description and schematic of a typical planar DBD actuator was presented in the previous section. In the current experiments electrodes are made of copper foil having thickness 0.035 mm. The width of the buried electrode is kept 20 mm and the width of the exposed electrode is 3 mm. A gap of 1 mm is maintained between the electrodes in the streamwise direction. The plasma starts from the end of the exposed electrode and covers the buried electrode width. Thus the plasma extent is 21 mm in the present study. The span of the electrodes (overlap) is kept 50 mm in the present study. The dielectric material used is Kepton tape. Five layers of Kepton tape separate the exposed and the buried electrode.

A device under the commercial name Miniplus4 generator was used to generate this high frequency (upto 30 kHz) high voltage AC. The input to this device is low DC voltage (25V), which is converted to AC at the low voltage board, controlled from PC using NI DAQ signal generation and control board. The voltage of the signal was stepped up by the transformer in the high voltage board to a voltage magnitude of the order of 25 kV, with a current of few mA. The high AC voltage, thus generated, is applied between the electrodes.

Smoke flow visualizations are carried out by seeding the DBD generated flow with smoke and illuminating the smoke particles with a planar laser sheet, so as to track the flow in the specific illuminated plane. A photograph of the setup is shown in Figure 3. The smoke is generated using incense sticks inside a reservoir (glass chamber). The smoke is pumped at very low speeds from the reservoir through a pipe, to a diffuser placed upstream of the DBD actuator. The diffuser slows down the smoke to almost stagnant condition at the location of the DBD actuator. A continuous laser source of 532 nm wavelength and 150 mW power is passed through a cylindrical lens to create the planar laser sheet.

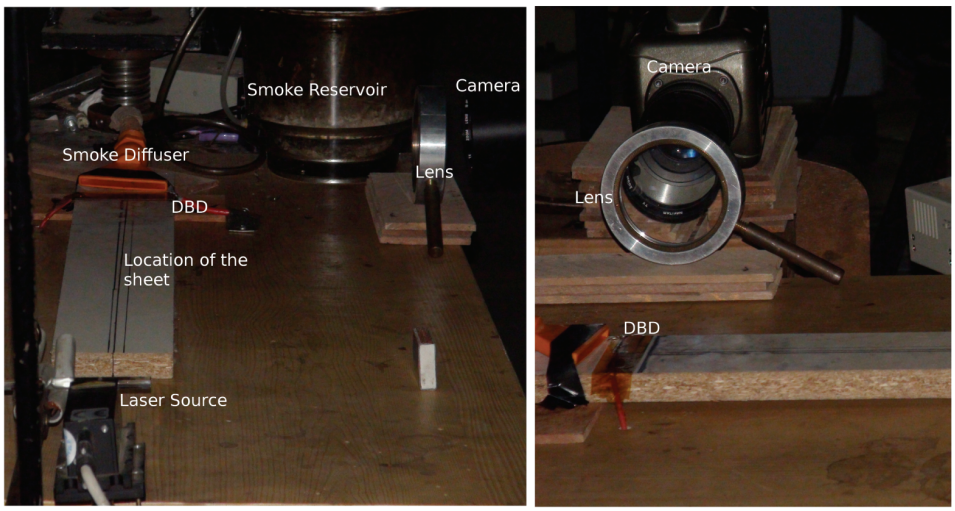

Figure 3. Photographs of the experimental setup for smoke flow visualization; Photo on left shows front view, on right shows side view

When the DBD actuator is switched on the smoke gets carried away with the flow, showing clearly the initial transients along the plane illuminated by laser. After the quasi-steady flow is established, the continuous pumping of the smoke ensures enough smoke availability to visualize the established flow. The visualizations are captured using a high speed camera, operated at a time resolution of 2000 frames per second, with spatial resolution of 800 x 600 pixels. An additional lens was used to resolve the flow better. The flow is visualized along the streamwise plane centered spanwise.

4. RESULTS AND DISCUSSIONS

4.1. Induced Wall Jet and Velocity Estimates

Time resolved smoke flow visualizations are able to capture the evolution of the flow from very close to the instant of starting the DBD; from the development of starting vortices to the established wall jet. Figure 4 shows the time evolution of the starting vortex captured using high speed camera operated at 2000 frames per second. During the initial frames the smoke carried away by the flow does not roll up, but rather move quite rapidly on the wall. Subsequently it rolls up indicating the formation of the starting vortex. The starting vortex moves with much slower velocities downstream (than the smoke front seen in initial frames) growing in diameter.

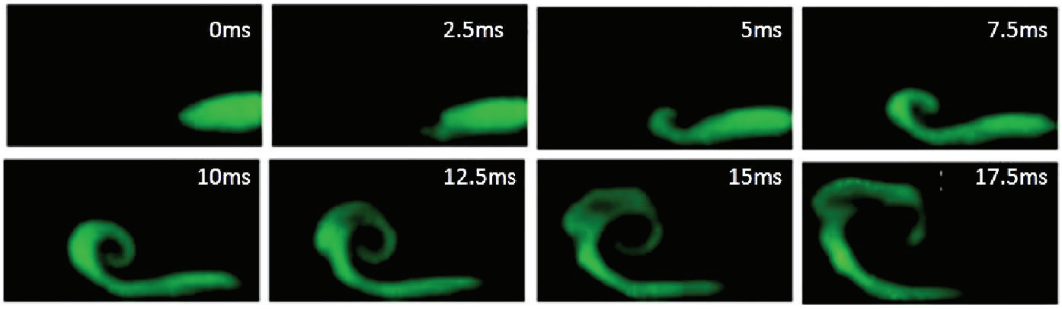

Figure 4. Smoke visualization of early stages of evolution of starting vortex

Clear smoke flow pictures (Figure 5) of the later stages show the starting vortex much downstream, with a larger diameter. The ensuing flow having K-H instability is also clearly visible. Figure 6 is of the established wall jet.

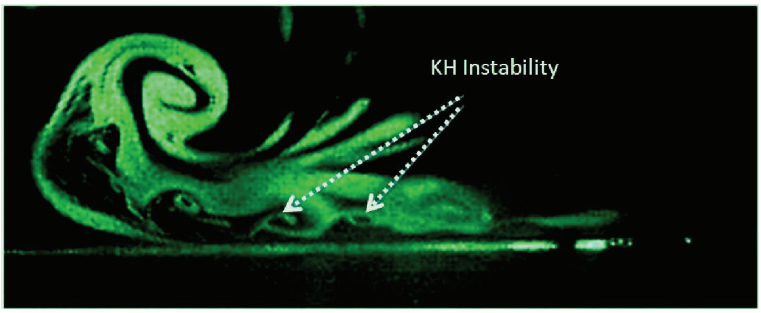

Figure 5. Smoke flow visualization of the starting vortex showing K-H instability

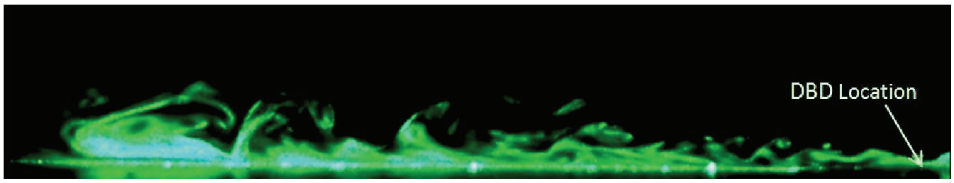

Figure 6. Smoke flow visualization of the established wall jet

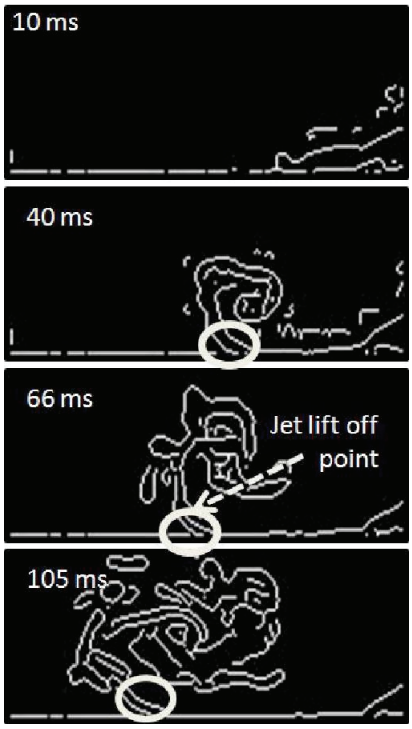

Figure 7. Processed smoke flow images showing the detected edges

Image processing allows quantitative information to be estimated from frames such as in Figure 4. Order of magnitude estimate for the velocity can be obtained from smoke flow visualizations. From these images the edges can be detected [22] and the jet lift off point is identified as the point where the lower edge of the jet starts to move away from the wall, as shown in Figure 7. During the initial frames there is no such lift off point. Rather there is end point of the smoke front in streamwise direction, whose motion can be tracked to find the velocity.

Before going for the visualization, the number of pixels occupied by a known reference length in the plane of observation is noted. From the number of pixels moved by the smoke front between two time frames, the velocity may be estimated. Two velocities are to be distinguished; one, the velocity of the streamwise end of the smoke front during the initial frames; the other, the velocity of the lift off point which characterizes the motion of the starting vortex. Smoke front moves substantially fast during the initial frames, and thus sweeps good number of pixels between two subsequent time frames of acquisition. Thus shorter time steps are enough to accurately estimate the velocity. Starting velocity is estimated to be around 5-8 m/s (dropping with time). The velocity of the lift off point on the other hand is much lower. Thus not many pixels are swept by the lift off point between subsequent frames of acquisition. The velocities are estimated with time steps, 5 times longer than that used in the estimation of starting velocity close to electrode. This can be better understood from Figure 8 which compares the lift off point velocity dependence on time for various time steps, from 1 to 8 frames of acquisition, a frame spacing corresponding to 0.5 ms.

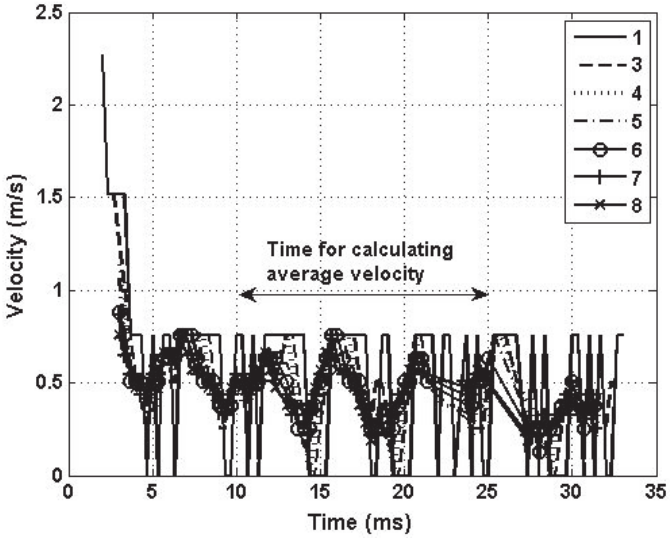

Figure 8. Comparison of velocity estimation of lift off point using different time steps

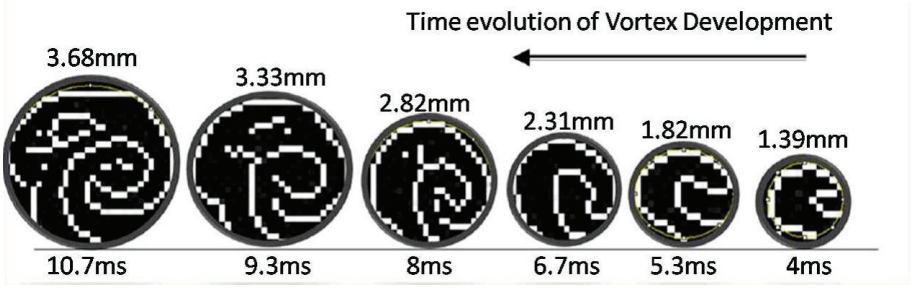

Figure 9. Growth of the diameter of starting vortex

Around 2.5 ms from the starting, the smoke starts to lift off and roll up. This velocity just before lift off is 2.3 m/s. From the 6th frame the lift off velocity is estimated. It can be seen from Figure 8 that velocity estimations are much better with longer time frames. From 10 to 25 ms the velocity of the lift off point is found to be around 0.5 m/s on an average. The motion and the velocity of the starting vortex, thus established are used as heuristic metric to illustrate the effect of various parameters on the behaviour of the actuator. The growth of the diameter of the starting vortex can also be estimated as shown in Figure 9.

4.2. Effect of AC Frequency

A linear increase of body force with AC frequency is often noted in the literature and this dependence is often used in phenomenological models as well [20]. Present experiments at different AC frequencies do not quite agree with that. Figure 10 shows the position of starting vortex at 50 ms after the start of actuation for different AC frequencies. It can be seen that the distance moved by starting vortex has progressively increased with frequency until 2 kHz where a maximum displacement is seen. From 2 kHz there is a reversal of the trend. It can be seen that at 4 kHz the starting vortex has moved smaller distance than that at even 1 kHz AC frequency. At 20 kHz no flow is seen. The behaviour can also be correlated with the visibility of plasma. Fig. 20 also shows the photographs of plasma taken from the top for the frequencies of 500 Hz, 2 kHz and 4 kHz, placed alongside the smoke flow visualization of the starting vortex. At 500 kHz the plasma is seen faintly. The plasma is seen most intense at 2 kHz and the intensity is relatively less at 4 kHz. At 20 kHz no plasma was seen. This means that the linear increase of body force with AC frequency may hold only within a certain range of AC frequency. Figure 11 showing the starting vortex speeds for different frequencies further clarifies this.

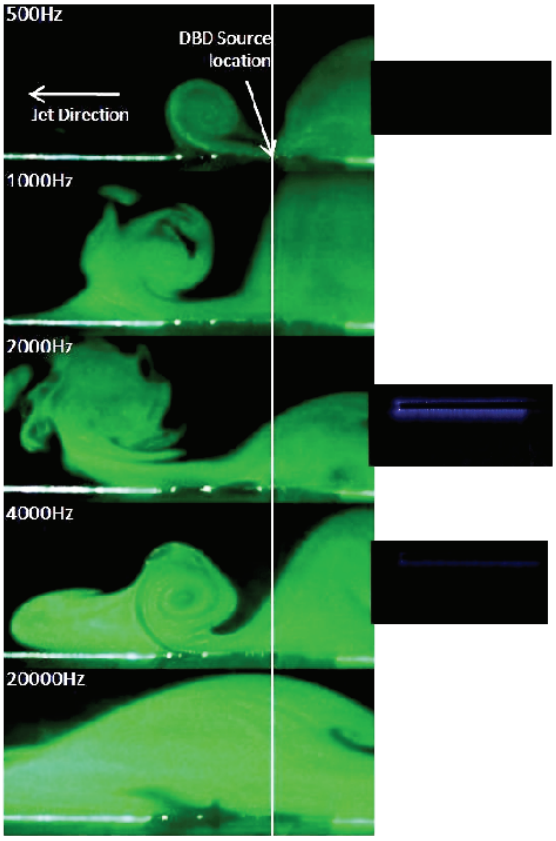

Figure 10. Comparison of starting vortex positions at 50 ms after the start of the actuation for different AC frequencies

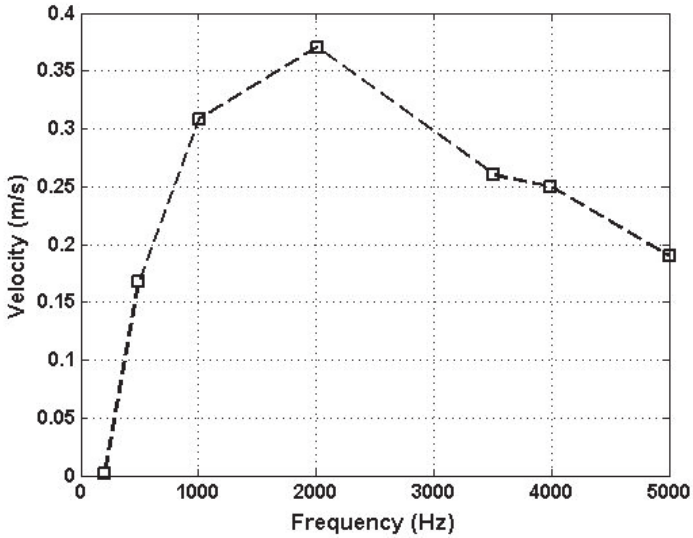

Figure 11. Dependence of starting vortex (lift off point) velocity with AC frequency

4.3. Pulsed Actuation

The DBD actuation can be pulsed by having the AC supply to the electrodes only for a fraction of a specified period of time. One can then distinguish from AC frequency, another frequency called modulating frequency associated with the specified time period. Duty cycle defines in terms of percentage, the fraction of time for which the supply power is on. This is better illustrated in Figure 12.

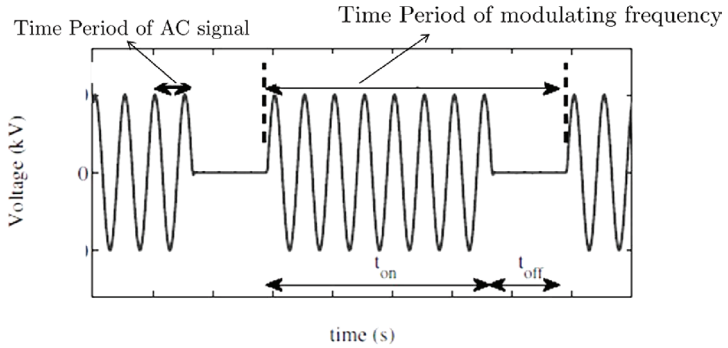

Figure 12. Illustration of modulating frequency and duty cycle

Operated in such pulsed fashion the DBD generates a starting vortex for each pulse. The starting vortex generated by each pulse follows the previous starting vortex as shown in Figure 13 for the case of 10% duty cycle and 10 Hz pulsing frequency.

Comparison of the motion of starting vortices (AC frequency of 2 kHz) for the case of start of steady actuation and for pulsed actuation at modulating frequency of 10 Hz with 2 different duty cycles of 50% and 10 % is shown in Figure 14. For the 100% duty cycle (steady actuation) after the starting vortex a steady wall jet is established, but with the pulsed cases starting vortices are generated during every cycle (associated with modulating frequency). For almost 75% of the time period the starting vortex with 50% duty cycle travels at same speed as that of 100% duty cycle case, after which the speed comes down. But by the time any difference in starting vortex speeds is noted (100 ms), the second starting vortex is generated at the start of the next cycle for the pulsed case. With 10% duty cycle a significant drop in starting vortex speed is seen, by around 50 ms (50% of the cycle). The pulsed actuation is expected to provide localized unsteady periodical disturbances. In that light the pulsed actuation at higher duty cycle seems to provide disturbances comparable in magnitude to that of steady actuation, and serve as well to provide oscillatory disturbance.

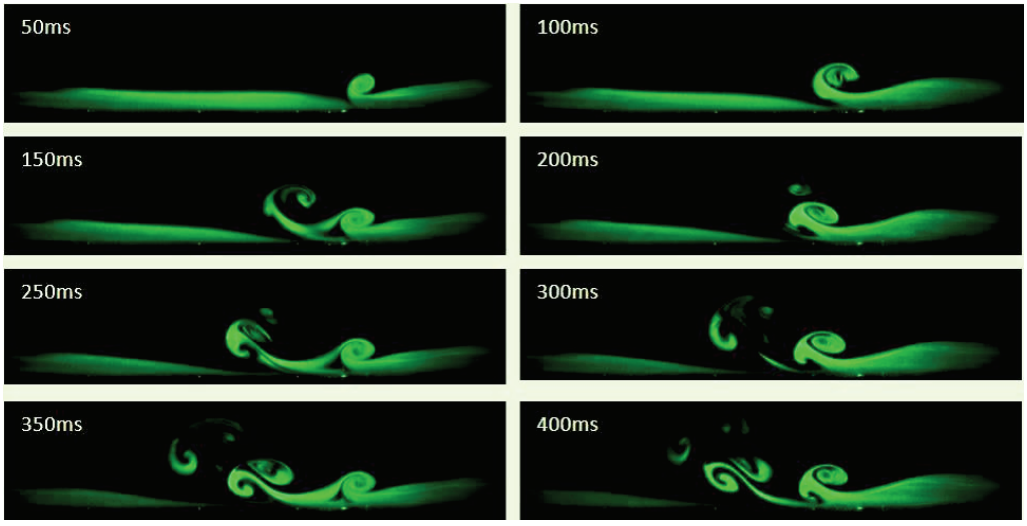

Figure 13. Sequence of vortices at 10 Hz pulsing frequency and 10 % duty cycle

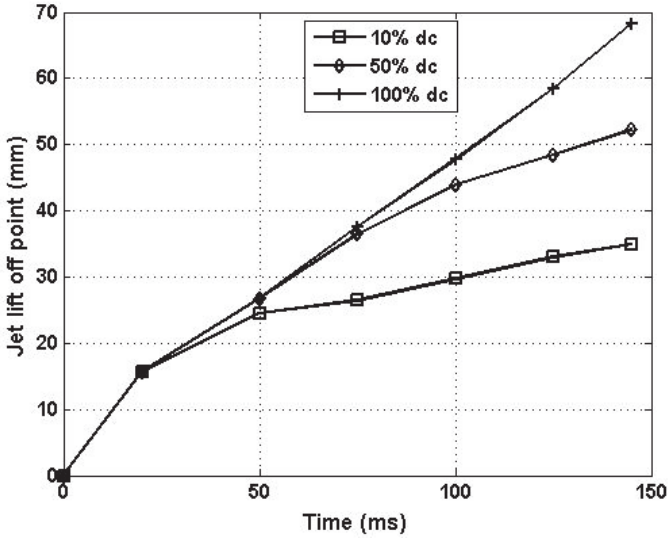

Figure 14. Comparison of starting vortex motion (in terms of the position of jet lift off point at given time) for different duty cycle at 10 Hz modulating frequency

5. CONCLUSIONS

DBD plasma actuation is investigated using time resolved smoke flow visualizations. The smoke flow visualizations are extended quantitatively to determine the velocity of the smoke front at the beginning of the DBD actuation and the velocity of the starting vortex. The DBD actuator is found to induce a maximum velocity of 8 m/s close to the electrode at AC frequency of 2 kHz. The estimated starting vortex velocity is then used to study the effect of AC frequency and pulsing of actuation. It is observed that the starting vortex velocity varies in nonlinear fashion with AC frequency. The starting vortex velocity increases with AC frequency till 2 kHz when it reaches a maximum and drops with further increase in AC frequency. The pulsed actuation at higher duty cycle is found to induce higher starting vortex velocity than at lower duty cycle.

REFERENCES

[1] T. C. Corke, C. L. Enloe and S. P. Wilkinson, Dielectric Barrier Discharge Actuators for Flow Control. *Annual Review of Fluid Mechanics*, 2010, 42, 505-529.

[2] M. L. Post and T. C. Corke, Separation control on high angle of attack airfoil using plasma actuators. *AIAA J*. 2004, 42, 2177.

[3] T. E. McLaughlin, M. D. Munska, J. P. Vaeth, T. E. Dauwalter, J. R. Goode, and S.G. Siegel, Plasma-based actuators for cylinder wake vortex control. AIAA Paper, 2004-2129.

[4] J. Huang, T. C. Corke, and F. O. Thomas, Plasma actuators for separation control of low pressure turbine blades. *AIAA Journal*, 2006, 44(1), 51–57.

[5] J. C. Little, High-Lift Airfoil Separation Control with Dielectric Barrier Discharge Plasma Actuators, PhD Thesis, The Ohio State University, 2010.

[6] R. A. Vincent, S. Larigaldie, P. Magre, and V. Sabel'nikov, Experimental study of a methane diffusion flame under dielectric barrier discharge assistance. *IEEE Transactions on Plasma Science 2007*, 35(2), 223–232.

[7] S. Chan, X. Zhang, and S. Gabriel, Attenuation of low-speed flow-induced cavity tones using plasma actuators. *AIAA Journal*, 2007, 45(7), 1525–1538.

[8] N. Benard, J. Bonnet, G. Touchard, and E. Moreau, Flow control by dielectric barrier discharge actuators - jet mixing enhancement. AIAA Paper, 2008-3878.

[9] S. Im, H. Do, and M. A. Cappelli, Dielectric barrier discharge control of a turbulent boundary layer in a supersonic flow. *Applied Physics Letters*, 2010, 97.

[10] M. Nishihara, K. Takashima, J. W. Rich, and I. V. Adamovich, Mach 5 bow shock control by a nanosecond pulse surface dielectric barrier discharge, *Physics of Fluids*, 2011, 23, 066101.

[11] C. L. Enloe, T. E. McLaughlin, R. D. VanDyken, K. D. Kachner, E. J. Jumper and T. C. Corke, Mechanisms and responses of a single dielectric barrier plasma actuator: plasma morphology, *AIAA Journal*, 2004, 42(3), 589-594.

[12] C. L. Enloe, T. E. McLaughlin, R. D. VanDyken, K. D. Kachner, E. J. Jumper, T. C. Corke, M. Post and O. Haddad, Mechanisms and responses of a single dielectric barrier plasma actuator: geometric effects, *AIAA Journal*, 2004, 42(3), 595-604.

[13] J. R. Roth and X. Dai, Optimization of the aerodynamic plasma actuator as an electro-hydrodynamic (EHD) electrical device, AIAA Paper, 2006-1203.

[14] F. O. Thomas, T. C. Corke, M. Iqbal, A. Kozlov and D. Schatzman, Optimization of dielectric barrier discharge plasma actuators for active aerodynamic flow control, *AIAA Journal*, 2009, 47(9), 2169-2178.

[15] M. Forte, J. Jolibois, J. Pons, E. Moreau, G. Touchard, and M. Cazalens, Optimization of a dielectric barrier discharge actuator by stationary and non-stationary measurements of the induced flow velocity: Application to airflow control, *Exp. Fluids*, 2007, 43, 917–928.

[16] J. Kriegseis, T. Dehler, S. Grundmann, and C. Tropea, Flowfield-characteristics generated by DBD plasma actuators, *A Dillmann et al (Eds): Numerical & Experimental Fluid Mechanics VII, NNFM 112*, 2010, 233–240.

[17] K. Singh and S. Roy, Force approximation for a plasma actuator operating in atmospheric air, *J. Appl. Phys*., 2008, 103.

[18] D. Orlov, Modeling and simulation of single dielectric barrier discharge plasma actuators, PhD Thesis, University of Notre Dame, 2006.

[19] Mertz and T. C. Corke, Single-dielectric barrier discharge plasma actuator modelling and validation, *J. Fluid. Mech*, 2010, 669, 557-583.

[20] W. Shyy, B. Jayaraman, and A. Anderson, Modeling of glow discharge induced fluid dynamics, *J Appl Phys*, 2002, 92, 6434–6443

[21] R.Whalley and K.Choi, "Starting, traveling, and colliding vortices: dielectric barrier discharge plasma in quiescent air", *Physics of Fluids*, 2010, 22

[22] J. Canny, A computational approach to edge detection, *IEEE Transactions on Pattern Analysis and Machine Intelligence*, 1986, PAMI-8 (6), 679-698.